LA-UR-15-27357 (Accepted Manuscript)

High-resolution in situ observations of electron precipitation-causing EMIC waves

Rodger, C
Hendry, A.
Cliverd, M
Kletzing, C
Brundell, j
Reeves, Geoffrey D.

To be published in: Geophysical Research Letters

DOI to publisher's version: 10.1002/2015GL066581

Permalink to record: http://permalink.lanl.gov/object/view?what=info:lanl-repo/lareport/LA-UR-15-27357

High-resolution In-situ Observations of Electron Precipitation-Causing EMIC Waves

Craig J. Rodger and Aaron T. Hendry

Department of Physics, University of Otago, Dunedin, New Zealand

Mark A. Clilverd

British Antarctic Survey (NERC), Cambridge, United Kingdom

Craig A. Kletzing

Department of Physics and Astronomy, University of Iowa, Iowa City, Iowa, United States of America

James B. Brundell

Department of Physics, University of Otago, Dunedin, New Zealand

Geoffrey D. Reeves

Space Science and Application Group, Los Alamos National Lab, Los Alamos, United States of America

Major Topic or Scientific Question: EMIC waves are thought to be highly important drivers of energetic electron loss from the radiation belt, however, there are very few experimental examples of precipitation-causing EMIC-events with limited measurements of the waves or precipitation.

New Scientific Knowledge: Here we have, for the first time, simultaneous in-situ measurements of the properties of the EMIC wave, the plasma conditions, and the precipitation fluxes for a case study event, as well as 4 additional examples of EMIC driven precipitation.

Broad Implications: There is increasing evidence of the importance of EMIC waves to radiation belt dynamics. However, the lack of experimental quantification of the waves &

precipitation means they are only roughly estimated in radiation belt models. We provide measurements.

Main point # 1: EMIC waves thought to be highly important drivers of electron loss from the outer radiation belt.

Main point # 2: To date there are few experimental examples of precipitation-causing EMIC-events.

Main point # 3: Simultaneous insitu measurements of EMIC wave, plasma, & precipitation flux provided for first time.

Abstract. Electromagnetic Ion Cyclotron (EMIC) waves are thought to be important drivers of energetic electron losses from the outer radiation belt through precipitation into the atmosphere. While the theoretical possibility of pitch angle scattering-driven losses from these waves has been recognized for more than 4 decades, there have been limited experimental precipitation observations to support this concept. We have combined satellite-based observations of the characteristics of EMIC waves, with satellite and ground-based observations of the EMIC-induced electron precipitation. In a detailed case study, supplemented by an additional 4 examples, we are able to identify for the first time the location, size, and energy range of EMIC-induced electron precipitation inferred from coincident precipitation data and relate them to the EMIC wave frequency, wave power, and ion-band of the wave as measured in-situ by the Van Allen Probes. These observations will better constrain modeling into the importance of EMIC wave-particle interactions.

1. Introduction

It has long been recognized that wave-particle interactions with Electromagnetic Ion Cyclotron (EMIC) waves are an important driver for precipitation of relativistic electrons [e.g., *Thorne and Kennel*, 1971; *Summers and Thorne*, 2003; *Thorne*, 2010]. EMIC waves are observed in the Pc1-Pc2 frequency range (0.1-5 Hz). Unstable ion ring distributions of tens to hundreds of keV ring current ions cause the waves to be generated near the magnetic equator propagating as left-handed circularly polarized waves, hence the term "Ion Cyclotron". Recent experimental studies have shown EMIC wave growth can occur at all local times and can persist for hours and sometimes even days [*Paulson et al.*, 2014; *Saikin et al.*, 2015]. Recent modeling studies have concluded that EMIC waves are very important sources of relativistic and ultra-relativistic electron losses from the outer radiation belt [e.g., *Drozdov et al*., 2015; *Ni et al.*, 2015].

Despite the decades of recognition that EMIC waves could be significant drivers of electron precipitation, until recently there has been little experimental evidence of this. However, some progress is now being made. Some of the earliest confirmation comes from ground-based measurements showing evidence of relativistic electron precipitation from subionospheric VLF and riometer observations along with the start of simultaneous EMIC waves in ground-based magnetometers [*Rodger et al.*, 2008]. Following on from this the properties of probable EMIC-wave precipitation events detected using the expected signature for EMIC-wave driven losses seen in low-Earth orbit satellite data have been presented [*Carson et al.*, 2012]. One of these probable EMIC-wave precipitation events was investigated in a case study using multiple ground-based experiments [*Clilverd et al.*, 2015], and was confirmed to be intense and EMIC-wave driven, but with unexpectedly low-energy cutoffs <400 keV similar to those suggested by *Hendry et al.* [2014]. At highly relativistic electron energies, indirect evidence of the efficiency of EMIC waves to drive losses has been

provided by Canadian ground-based magnetometer data and >2.3 MeV trapped relativistic electron from the Van Allen probes [*Usanova et al.*, 2014]. Thus, although there is increasing evidence of electron precipitation from EMIC waves, the detailed characteristics of the precipitation and associated waves remain uncertain.

However, there are many examples in the literature where EMIC waves are observed on the ground or in space for which there appear to be no electron precipitation occurring, even when the measurements are available [e.g., *Usanova et al.*, 2014; *Engebretson et al.*, 2015]. There is also growing recent experimental evidence which suggest that EMIC-waves may precipitate electrons with energies as low as a few hundred keV [*Hendry et al.*, 2014; *Clilverd et al.*, 2015; *Blum et al.*, 2015] rather than the relativistic energies which are widely produced in theoretical modeling [e.g., *Meredith et al.*, 2003; *Chen et al.*, 2011; *Usanova et al.*, 2014]. There is some theoretical support for such comparatively low energy thresholds for EMIC-driven electron precipitation. The minimum resonant energy for a He-band EMIC wave inside the plasmasphere was shown to be as low as ~100 keV for waves at ~1 Hz [*Omura and Zhao*, Fig.2, 2013] and some quasi-linear theory has indicated minimum resonance energies of ~300-400 keV [*Summers and Thorne*, 2003; *Ukhorskiy et al.*, 2010].

In order to better constrain modeling and understand the importance of EMIC wave-particle interactions it is necessary to have in-situ observations of the wave and plasma characteristics for EMIC waves which are confirmed to be driving electron precipitation. In this paper we provide in-situ observations supported by ground-based precipitation measurements to fulfill this goal. We provide a detailed description of one event, identifying for the first time the location, size, and energy range of EMIC-induced electron precipitation caused by waves with in-situ measurements of EMIC wave frequency, wave power, and ion-band. We also provide the wave and plasma parameters for 4 other similar events.

2. Experimental Datasets

98 **2.1 Van Allen Probes Observations**

99 We make use of multiple experiments onboard the Van Allen Probes, in particular the
100 magnetometer and ELF-VLF and LF observations from the Electric and Magnetic Field
101 Instrument Suite and Integrated Science (EMFISIS) [*Kletzing et al.*, 2013], including the cold
102 plasma densities measurements [*Kurth et al.*, 2015]. EMFISIS provides observations of the
103 EMIC waves as well as the geomagnetic field intensities. Pitch-angle resolved electron fluxes
104 are provided by the Magnetic Electron Ion Spectrometer (MagEIS) [*Blake et al.*, 2013] and
105 the Relativistic Electron-Proton Telescope (REPT) [*Baker et al.*, 2013] instruments.

106

107 **2.2 Low Earth Orbit Precipitation Observations**

108 One source of precipitation observations comes from the Medium Energy Proton and
109 Electron Detector (MEPED) instrument onboard the Polar-orbiting Operational
110 Environmental Satellite (POES) [*Evans and Greer*, 2004]. This dataset is unusual in that it
111 measures precipitation electron fluxes inside the bounce loss cone. The characteristics of the
112 POES electron precipitation measurements have been comprehensively described in the
113 literature [e.g., *Rodger et al.*, 2010a,b; *Carson et al.*, 2012].

114

115 **2.3 Ground-based Observations**

116 The other source of precipitation observations comes from narrow band subionospheric
117 very low frequency (VLF) sites that are part of the Antarctic Arctic Radiation-belt dynamic
118 deposition VLF Atmospheric Research Konsortia (AARDDVARK) network [*Clilverd et*
119 *al.,* 2009; for further information see the description of the array at
120 www.physics.otago.ac.nz/space/AARDDVARK_homepage.htm]. Subionospheric VLF
121 responds to electron precipitation which penetrates beneath the lower boundary of the
122 ionosphere, that is electrons with minimum detectable electron precipitation energies of
123 ~150 keV (day) and ~50 keV (night) [*Rodger et al.*, 2012].

124 **3. EMIC Event on 24 September 2013 - Wave Activity**

125 Figure 1 presents a set of spectrograms showing an EMIC event which started at 16:42 UT
126 on 24 September 2013 observed by EMIFISIS onboard RBSP-A. The upper 3 spectrograms
127 are the 3 components of the magnetic field in GSM coordinates. The lower panel of this
128 figure shows the variation in the magnitude of the geomagnetic field, also observed by the
129 EMIFISIS magnetometer. Shortly before the onset of the EMIC wave the geomagnetic field
130 changes, with the magnitude of the total field altering by ~30 nT in 4 minutes from
131 16:40 UT. This change can also be seen in the He and O ion gyrofrequencies which are
132 plotted as white lines in the spectrogram panels. It is likely that this magnetic field
133 compression triggered the underlying instability that produced the wave, as has been
134 previously observed across a wide range of MLT (see the discussion in *Engebretson et al.*
135 [2015]).

136 This is a fairly strong and clear example of a He-band EMIC wave event. A summary of
137 the wave and plasma properties determined from the EMFISIS observations of this event
138 are given in Table 1, which shows that this event occurred in the afternoon sector and inside
139 the plasmasphere, although it is likely to have been close to the plasmapause given the
140 electron density value.

141 The upper panel of Figure 2 shows a spectrogram of the EMFISIS magnetic field ELF and
142 VLF observations from RBSP-A across the same time period as shown in Figure 1. Here the
143 spectrograms of the summed magnetic field components have been taken. The lower panel
144 of this figure is the wave-normal angle for the observations shown in the upper panel.
145 Typically, signals with wave normal angles <45° are likely to be whistler mode waves,
146 while those >75° would be indicative of magnetosonic waves [*Gurnett and Bhattacharjee*,
147 2005] that are restricted to the region of the geomagnetic equator. Figure 2 indicates that the
148 ELF-VLF wave activity in the time period considered is quiet. Around this time there is a
149 ~100-200 Hz magnetosonic wave that is fading out, as well as a weak ~50-90 Hz

150 magnetosonic wave which starts around the time of the magnetospheric compression.
151 Whistler mode wave activity is weak, particularly in the time period of the strong EMIC
152 wave. It is well known that whistler mode waves can pitch angle scatter electrons and cause
153 precipitation [e.g. *Thorne*, 2010], whereas magnetosonic waves are up to two orders of
154 magnitude less effective at driving precipitation [*Shprits et al.*, 2013]

155 **4. Precipitation Observations**

156 **4.1 AARDDVARK**

157 At 16:42 UT the northern hemisphere footprint of the RBSP-A spacecraft was located near
158 Iceland. We have examined AARDDVARK data at this time, concentrating on Atlantic-
159 longitude observations in the region of the RBSP-A observations. The upper two panels of
160 Figure 3 show examples of the AARDDVARK observations made from St John's, Canada
161 (STJ, red line) and Reykjavik, Iceland (REK, blue line). The amplitude and phase
162 perturbations for two transmitters are plotted, with callsign NRK (red line in the Figure,
163 located in Iceland) and NDK (blue line, located in North Dakota, USA). Figure 3 presents
164 the change in amplitude in phase relative to undisturbed conditions, i.e., the change relative
165 to the quiet day curve. There are clear amplitude perturbations starting at 16:42 UT (marked
166 by the dashed vertical line). We observe consistent evidence of subionospheric
167 perturbations beginning at the start time of the RBSP-observed EMIC wave seen in Figure
168 1. As there is no significant whistler mode wave activity occurring at this time (as shown in
169 Figure 2), the EMIC wave is the most likely candidate for driving the electron precipitation
170 causing the observed AARDDVARK precipitation.

171 The lower panel of Figure 3 shows a geographic map of the AARDDVARK paths
172 analyzed in this study. Note that there is both an AARDDVARK receiver and a VLF
173 transmitter in Iceland, with the NRK transmitter symbol largely obscured. In this plot

AARDDVARK paths which were seen to respond to precipitation at the EMIC wave start time are shown in green, while the unresponsive paths are shown as dashed light blue lines.

The AARDDVARK observations are clearly consistent with precipitation occurring near Iceland around the *L*-shells of the RBSP-footprint. The size of the precipitation patch is sufficiently wide enough that transmitter receiver paths to the immediate east and west of Iceland are affected, but not so wide to affect those paths from Western European transmitters to Finland, or from NPM to the Antarctic station, Halley. The observed region of the EMIC-driven precipitation covers ~13-17 MLT.

4.2 POES Observations

Near the start of the period during which the EMIC wave was observed by RBSP-A, there was a serendipitous conjunction with NOAA-15, one of the POES satellites that have been extensively used to investigate radiation belt precipitation. The orbital track of NOAA-15 passed from south to north at the eastern edge of Iceland. At 16:41:55 UT the MEPED instrument onboard this satellite observed a burst of proton and electron precipitation with the signature expected from EMIC waves [*Sandanger et al.*, 2009], detected by an automatic algorithm [*Carson et al.*, 2012]. Such precipitation triggers have recently been shown to be associated with observed EMIC waves [Hendry, A. T., C. J. Rodger, M. A. Clilverd, M. J. Engebretson, M. R. Lessard, I. R. Mann, T. Raita, and D. K. Milling, First large scale survey of POES-detected EMIC wave driven energetic electron precipitation, *J. Geophys. Res.*, (in preparation), 2015.]. The location of this algorithm-trigger event is shown as the blue star in Figure 3, very close to the eastern end of the RBSP-A atmospheric footprint. As this observation was made at essentially the same location and time as the start of the RBSP-A EMIC wave observation, the precipitation includes both protons and a strong relativistic component as expected for effective EMIC-wave scattering, and RBSP-A

reports no significant ELF/VLF wave activity, we assume the POES precipitation event was produced by the observed EMIC wave.

The precipitation spike has been analyzed as described in section 3.2 of *Clilverd et al.* [2015]. By using the proton and electron precipitation measurements and a detailed understanding of the instrument response [*Yando et al.*, 2011], one can determine an energy spectrum, flux magnitude, and energy cutoff estimations for the observed precipitation. This precipitation event is best fit with a power-law, with spectral gradient values from -2.7 to -1.7, lower energy precipitation cutoffs of 140-230 keV, upper cutoff estimates of 1.6-8 MeV, and precipitation magnitudes of ~1.25×10^4 $cm^{-2}sr^{-1}s^{-1}$.

4.3 AARDDVARK Modeling

The location of the POES trigger event and the RBSP-A footprints provide useful constraints on the likely longitudinal range of the precipitation affecting the paths from GQD and DHO to Iceland, i.e., the transmitters to the east of the Reykjavik receiver. We undertake modeling of the subionospheric perturbations predicted from precipitation defined by the POES energy and power-law gradient, using approaches previously described [e.g., *Rodger et al.*, 2012; *Clilverd et al.*, 2015].

We find that the modeling is sensitive to the initial conditions, for example comparatively small changes in the starting location of the energetic electron precipitation change along the path (i.e., changes of tens of km). This is likely due to the relatively short, all sea path from the transmitter to receiver, such that there is a high number of significant modes present in the Earth ionosphere waveguide, and also the small ionospheric region affected. Our modeling of the perturbations observed on the transmissions from DHO (ΔAmplitude=+1.8 dB, ΔPhase=-3°) and GQD (ΔAmplitude=+0.6 dB, ΔPhase=-3°), at the EMIC-wave onset time, indicates these changes are consistent with the effect caused by imposing the POES precipitation observations, i.e. flux magnitudes of ~1×10^4 $cm^{-2}sr^{-1}s^{-1}$.

225 The modeling reproduces the observations for power law gradients which have low energy
226 cutoffs, i.e. ~200 keV. It was not possible to successfully model the subionospheric VLF
227 perturbations using low energy cutoffs of ~1 MeV. Such cutoffs produce much larger
228 amplitude and phase perturbations than observed. Therefore, the AARDDVARK
229 observations confirm the POES satellite flux and energy cutoffs.

230 **5. Trapped Electron Flux Observations**

231 Figure 4 shows the RBSP-A MagEIS pitch angle resolved trapped fluxes with 1 MeV
232 (upper panel) and 225 keV energies (lower panel). At the time of the magnetospheric
233 compression and the start of the EMIC wave the fluxes change to a butterfly distribution,
234 with s a 50% decrease in the 90° pitch angles fluxes from 16:41-16:44 UT. A similar
235 signature is seen in the MagEIS fluxes at energies >143 keV, and in REPT fluxes
236 ≤2.6 MeV. The REPT fluxes >2.6 MeV are at noise levels. There is no evidence of
237 significantly different behavior between the 2.6 MeV fluxes and those at lower energies, in
238 apparent contradiction to the conclusions of *Usanova et al.* [2014], although this could be
239 obscured by the changes leading to the butterfly distribution.

240 Such butterfly distributions can be produced by magnetopause shadowing or by field line
241 stretching and drift shell splitting [e.g., *Roederer et al.*, 1970; *Sibeck et al.*, 1987]. However,
242 this does not explain the observations in our case, due to the small time dispersion between
243 the energies. The source of the distribution should be only ~0.6 MLT away to be consistent
244 with the energy dispersion observed (i.e., located at ~16 MLT). While we note that the
245 butterfly distribution is unlikely to be caused by magnetopause shadowing, there has not
246 been evidence suggesting such pitch angle distributions can be produced by EMIC waves.
247 Nonetheless, the change to this distribution makes it essentially impossible to see evidence
248 of the pitch angle scattering driving the observed precipitation.

249 **6. Additional Events**

In our examination of RBSP-A EMIC wave data and comparison with precipitation data we found 4 other events in which RBSP-A observed an EMIC wave, there was little evidence of confounding ELF/VLF whistler-mode wave activity, and AARDDVARK sites at Churchill (Canada), Fairbanks (Alaska), and Sodankylä (Finland) confirmed the presence of energetic electron precipitation. The RBSP-A in-situ measurements of EMIC wave and plasma parameters for these 4 additional events, along with those for 24 September 2013, are given in Table 1. All of these 5 events have butterfly distributions in the MagEIS trapped electron fluxes which begin near the wave start time.

In the current study we have chosen to concentrate on the analysis of the 24 September 2013 event, due to the serendipitous conjunctions between RBSP-A, NOAA-15, and AARDDVARK network observations. None of the other events listed in Table 1 have such close conjunctions. We note that there are multiple POES-triggers on 27 August 2013, and that the events on this day may deserve more attention in a future study.

7. Summary

For the first time we have combined satellite-based observations of the characteristics of EMIC waves, with satellite and ground-based observations of the EMIC-induced electron precipitation. In a detailed case study, supplemented by an additional 4 examples, we are able to identify the location, size, energy range of EMIC-induced electron precipitation inferred from coincident POES/AARDDVARK data and relate them to the EMIC wave frequency, PSD wave power, and ion-band as measured by the Van Allen Probes.

We find that:

1. We find that the precipitation-causing EMIC waves typically occur over the MLT range 16-00 UT, and at L~5.4+/-0.4. The background plasmaspheric electron densities are ~100 el/cc, suggesting waves that are located close to the plasmapause. The frequency of

the EMIC waves are typically 0.3-0.5 Hz, and are mostly found within the helium band. The typical wave power spectral density is ~1 nT^2/Hz, with peak powers ~10 times higher.

2. The EMIC-induced electron precipitation was detected by the ground-based AARDDVARK network, with one coincident measurement made by one of the NOAA POES satellites. The region of electron precipitation was small in geomagnetic latitude, i.e., <50 km (ΔL=0.15), but high in flux, i.e., ~10^4 $cm^{-2}sr^{-1}s^{-1}$, with a power law energy spectrum beginning at ~200 keV. Radio wave propagation modeling of the AARDDVARK observations are supportive of the POES detection of a narrow latitudinal precipitation patch, as well as extended in longitude through several hours of MLT, and occurring at the time of the EMIC wave observed by RBSP.

Acknowledgments. The authors would like to thank Richard Yeo for hosting the AARDDVARK receiver in Reykjavik, the following institutional AARDDVARK hosts: Churchill Northern Studies Center USGS/Magnetic Observatories Fairbanks, and Sodankylä Geophysical Observatory. We would also like to acknowledge the researchers and engineers of NOAA's Space Environment Center for the provision of the data and the operation of the SEM-2 instrument carried onboard these spacecraft, the many teams involved in the Van Allen Probes, and the developers of the Autoplot interactive data tool. The research at University of Iowa was supported by JHU/APL contract 921647 under NASA prime contract NAS5-01072.

Data availability is described at the following websites: http://rbspgway.jhuapl.edu/ (Van Allen Probes Science Gateway), http://emfisis.physics.uiowa.edu/ (EMFISIS), http://www.rbsp-ect.lanl.gov/data_pub/rbspa/mageis/level3/ (MagEIS), http://www.rbsp-ect.lanl.gov/data_pub/rbspb/rept/level3/ (REPT), http://www.rbsp-ect.lanl.gov/data_pub/rbspa/MagEphem/def/2013/ (MegEphem),

http://satdat.ngdc.noaa.gov/sem/poes/data/ (POES SEM-2), http://www.physics.otago.ac.nz/space/AARDDVARK_homepage.htm (AARDDVARK).

References

Baker, J. B., et al. (2013), The Relativistic Electron-Proton Telescope (REPT) Instrument on Board the Radiation Belt Storm Probes (RBSP) Spacecraft: Characterization of Earth's Radiation Belt High-Energy Particle Populations, Space Sci. Rev., 179, 337–381, 10.1007/s11214-012-9950-9.

Blake, J. B., et al. (2013), The magnetic electron ion spectrometer (MagEIS) instruments aboard the radiation belt storm probes (RBSP) spacecraft, Space Sci. Rev., 179, 383–421, doi:10.1007/s11214-013-9991-8.

Blum, L. W., A. Halford, R. Millan, J. W. Bonnell, J. Goldstein, M. Usanova, M. Engebretson, M. Ohnsted, G. Reeves, H. Singer, et al. (2015), Observations of coincident EMIC wave activity and duskside energetic electron precipitation on 18–19 January 2013, Geophys. Res. Lett., 42, 5727–5735, doi:10.1002/2015GL065245.

Carson, B. R., C. J. Rodger, and M. A. Clilverd (2012), POES satellite observations of EMIC-wave driven relativistic electron precipitation during 1998–2010, J. Geophys. Res. Space Physics, 118, 232–243, doi:10.1029/2012JA017998.

Clilverd, M. A., C. J. Rodger, N. R. Thomson, J. B. Brundell, Th. Ulich, J. Lichtenberger, N. Cobbett, A. B. Collier, F. W. Menk, A. Seppälä, P. T. Verronen, and E. Turunen (2009), Remote sensing space weather events: the AARDDVARK network, Space Weather, 7, S04001, doi:10.1029/2008SW000412.

Clilverd, M. A., R. Duthie, R. Hardman, A. T. Hendry, C. J. Rodger, T. Raita, M. Engebretson, M. R. Lessard, D. Danskin, and D. K. Milling (2015), Electron precipitation from EMIC waves: A case study from 31 May 2013. J. Geophys. Res. Space Physics, 120, 3618–3631. doi: 10.1002/2015JA021090.

Drozdov, A. Y., Y. Y. Shprits, K. G. Orlova, A. C. Kellerman, D. A. Subbotin, D. N. Baker, H. E. Spence, and G. D. Reeves (2015), Energetic, relativistic, and ultrarelativistic electrons: Comparison of long-term VERB code simulations with Van Allen Probes measurements. J. Geophys. Res. Space Physics, 120, 3574–3587. doi: 10.1002/2014JA020637.

330 Engebretson, M. J., et al. (2015), Van Allen probes, NOAA, GOES, and ground observations
331 of an intense EMIC wave event extending over 12 h in magnetic local time, J. Geophys.
332 Res. Space Physics, 120, doi:10.1002/2015JA021227.
333 Gurnett, D. A., and A. Bhattacharjee (2005), Introduction to Plasma Physics: With Space and
334 Laboratory Applications, Cambridge Univ. Press, New York.
335 Hendry, A. T., C. J. Rodger, B. R. Carson, and M. A. Clilverd (2014), Investigating the upper
336 and lower energy cutoffs of EMIC-wave driven precipitation events, pp. 4, IEEE Xplore,
337 doi: 10.1109/URSIGASS.2014.6929964.
338 Hendry, A. T., C. J. Rodger, M. A. Clilverd, M. Engebretson, M. R. Lessard, I. Mann, T.
339 Raita, and D. Milling, First large scale survey of POES-detected EMIC wave driven
340 energetic electron precipitation, J. Geophys. Res., (in preparation), 2015.
341 Kletzing, C. A., et al. (2013), The electric and magnetic field instrument suite and integrated
342 studies (EMFISIS) on RBSP, Space Sci. Rev., 179, 127–181.
343 Kurth, W. S., De Pascuale, S., Faden, J. B., Kletzing, C. A., Hospodarsky, G. B., Thaller, S.
344 and Wygant, J. R. (2015), Electron densities inferred from plasma wave spectra obtained
345 by the Waves instrument on Van Allen Probes. J. Geophys. Res. Space Physics, 120: 904–
346 914. doi: 10.1002/2014JA020857.
347 Mauk, B. H., N. J. Fox, S. G. Kanekal, R. L. Kessel, D. G. Sibeck, A. Ukhorskiy (2013),
348 Science Objectives and Rationale for the Radiation Belt Storm Probes Mission, Space Sci.
349 Rev., Vol. 179, 3-27, doi:10.1007/s11214-012-9941-x.
350 Meredith, N. P., R. M. Thorne, R. B. Horne, D. Summers, B. J. Fraser, and R. R. Anderson
351 (2003), Statistical analysis of relativistic electron energies for cyclotron resonance with
352 EMIC waves observed on CRRES, J. Geophys. Res., 108, 1250,
353 doi:10.1029/2002JA009700, A6.
354 Ni, B., X. Cao, Z. Zou, C. Zhou, X. Gu, J. Bortnik, J. Zhang, S. Fu, Z. Zhao, R. Shi, et al.
355 (2015), Resonant scattering of outer zone relativistic electrons by multi-band EMIC waves
356 and resultant electron loss timescales, J. Geophys. Res. Space Physics, 120,
357 doi:10.1002/2015JA021466.
358 Omura, Y., and Q. Zhao (2013), Relativistic electron microbursts due to nonlinear pitch angle
359 scattering by EMIC triggered emissions, J. Geophys. Res. Space Physics, 118, 5008–5020,
360 doi:10.1002/jgra.50477.
361 Paulson, K. W., C. W. Smith, M. R. Lessard, M. J. Engebretson, R. B. Torbert, and C. A.
362 Kletzing (2014), In Situ Observations of Pc1 Pearl Pulsations by the Van Allen Probes,
363 Geophys. Res. Lett., 41, doi:10.1002/2013GL059187.

364 Roederer, J. G. (1970), Dynamics of Geomagnetically Trapped Radiation, Springer, New
365 York.
366 Rodger, C. J., B. R. Carson, S. A. Cummer, R. J. Gamble, M. A. Clilverd, J-A. Sauvaud, M.
367 Parrot, J. C. Green, and J.-J. Berthelier (2010b), Contrasting the efficiency of radiation
368 belt losses caused by ducted and non-ducted whistler mode waves from ground-based
369 transmitters, J. Geophys. Res., 115, A12208, doi:10.1029/2010JA015880.
370 Rodger, C. J., M. A. Clilverd, A. J. Kavanagh, C. E. J. Watt, P. T. Verronen, and T. Raita
371 (2012), Contrasting the responses of three different ground-based instruments to energetic
372 electron precipitation, Radio Sci., 47, RS2021, doi:10.1029/2011RS004971.
373 Rodger, C. J., M. A. Clilverd, J. C. Green, and M. M. Lam (2010a), Use of POES SEM-2
374 observations to examine radiation belt dynamics and energetic electron precipitation into
375 the atmosphere, J. Geophys. Res., 115, A04202, doi: 10.1029/2008JA014023.
376 Rodger, C. J., T. Raita, M. A. Clilverd, A. Seppälä, S. Dietrich, N. R. Thomson, and T. Ulich
377 (2008), Observations of relativistic electron precipitation from the radiation belts driven
378 by EMIC waves, Geophys. Res. Lett., 35, L16106, doi:10.1029/2008GL034804.
379 Saikin, A. A., J.-C. Zhang, R. C. Allen, C. W. Smith, L. M. Kistler, H. E. Spence, R. B.
380 Torbert, C. A. Kletzing, and V. K. Jordanova (2015), The occurrence and wave properties
381 of H+-, He+-, and O+-band EMIC waves observed by the Van Allen Probes, J. Geophys.
382 Res. Space Physics, 120, doi:10.1002/2015JA021358.
383 Sandanger, M., F. Søraas, M. Sørbø, K. Aarsnes, K. Oksavik, and D. Evans (2009),
384 Relativistic electron losses related to EMIC waves during CIR and CME storms, Journal
385 of Atmospheric and Solar-Terrestrial Physics, 71 (10-11), 1126 – 1144,
386 doi:10.1016/j.jastp.2008.07.006.
387 Shprits Y. Y., A. Runov, and B. Ni (2013), Gyro-resonant scattering of radiation belt
388 electrons during the solar minimum by fast magnetosonic waves, J. Geophys. Res. Space
389 Physics, 118, 648–652, doi:10.1002/jgra.50108.
390 Sibeck, D. G., R. W. McEntire, A. T. Y. Lui, R. E. Lopez, and S. M. Krimigis (1987),
391 Magnetic field drift shell splitting: Cause of unusual dayside particle pitch angle
392 distributions during storms and substorms, J. Geophys. Res., 92(A12), 13485–13497,
393 doi:10.1029/JA092iA12p13485.
394 Summers, D., and R. M. Thorne (2003), Relativistic electron pitch-angle scattering by
395 electromagnetic ion cyclotron waves during geomagnetic storms, J. Geophys. Res., 108,
396 1143, doi:10.1029/2002JA009489, A4.

Thorne, R. M. (2010), Radiation belt dynamics: The importance of wave-particle interactions, Geophys. Res. Lett., 37, L22107, doi:10.1029/2010GL044990.

Thorne, R. M., and C. F. Kennel (1971), Relativistic electron precipitation during magnetic storm main phase, J. Geophys. Res., 76, 4446, doi:10.1029/JA076i019p04446.

Ukhorskiy, A. Y., Y. Y. Shprits, B. J. Anderson, K. Takahashi, and R. M. Thorne (2010), Rapid scattering of radiation belt electrons by storm-time EMIC waves, Geophys. Res. Lett., 37, L09101, doi:10.1029/2010GL042906.

Usanova, M. E., et al. (2014), Effect of EMIC waves on relativistic and ultrarelativistic electron populations: Groundbased and Van Allen Probes observations, Geophys. Res. Lett., 41, doi:10.1002/2013GL059024.

Yando, K., R. M. Millan, J. C. Green, and D. S. Evans (2011), A Monte Carlo simulation of the NOAA POES Medium Energy Proton and Electron Detector instrument, J. Geophys. Res., 116, A10231, doi:10.1029/2011JA016671.

M. A. Clilverd, British Antarctic Survey (NERC), High Cross, Madingley Road, Cambridge CB3 0ET, England, U.K. (e-mail: macl@bas.ac.uk).

J. B. Brundell, A. T. Hendry and C. J. Rodger, Department of Physics, University of Otago, P.O. Box 56, Dunedin, New Zealand. (email: james@brundell.co.nz, aaron.hendry@otago.ac.nz, crodger@physics.otago.ac.nz).

C. A. Kletzing, Department of Physics and Astronomy, University of Iowa, Iowa City, Iowa, U.S.A. (email: craig-kletzing@uiowa.edu)

Geoffrey D. Reeves, Space Science and Application Group, Los Alamos National Lab, Los Alamos, U.S.A. (email: reeves@lanl.gov)

424

Date Time (UT)	24-Sep-13 16:41	24-Mar-13 6:57	14-Aug-13 4:57	27-Aug-13 15:52	27-Aug-13 16:52
L	5.1	5.7	5.3	5.3	5.8
MLT	16.5	23.7	18.1	17.9	18.7
f_{upper} (Hz)	0.5	0.9	0.2	0.55	0.35
f_{lower} (Hz)	0.25	0.3	0.4	0.47	0.15
PSD wave power					
typical (nT^2/Hz)	0.8	0.1	3	0.3	0.3
peak (nT^2/Hz)	10	1	42	2	6
N_e (cm^{-3})	190	79	63	112	43
f_{pe} (kHz)	120	80	72	95	58
f_{ce} (kHz)	5.5	3.9	4.3	4.9	3.1
RBSP satellite	A	B	B	A	A
Ion Band	He	H	He	He	He

425

426 **Table 1.** Properties at the times of the observed EMIC wave driven precipitation events.
427 The first event is that described in detail in this study. The parameters listed are as measured
428 by RBSP-A. f_{upper}, f_{lower}: upper and lower EMIC wave frequency, PSD: EMIC wave power
429 spectral density, N_e: cold electron density, f_{pe}: electron plasma frequency, f_{ce}: electron gyro-
430 frequency.

431

432

433

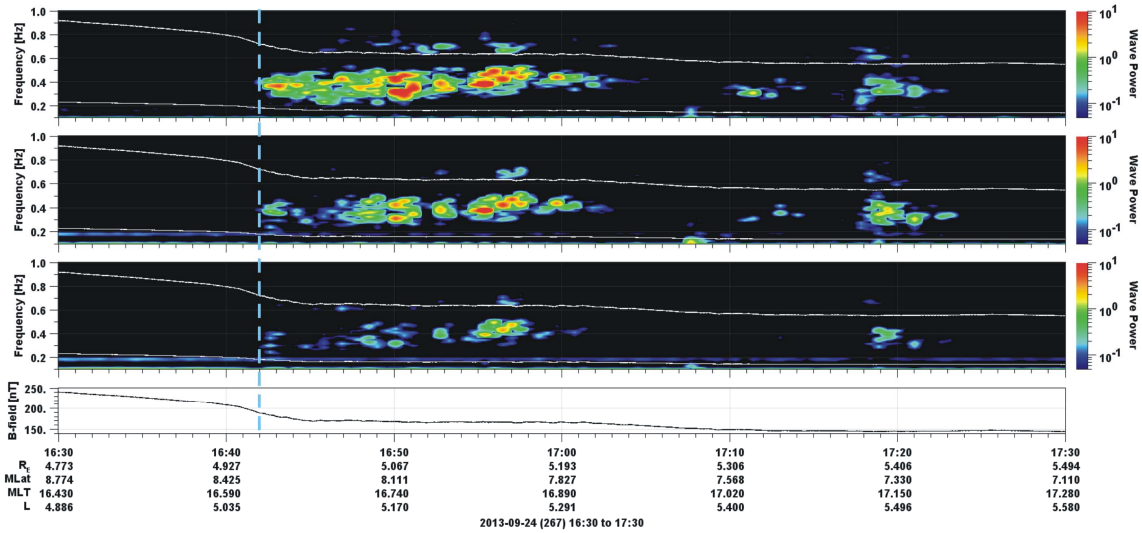

434

435 **Figure 1.** The three upper panels show spectrograms of the 3 components of the magnetic
436 field in GSM coordinates from the EMFISIS experiment onboard RBSP-A on 24 September
437 2013. Wave power has units of nT^2/Hz. The white lines show the local ion gyrofrequencies
438 for He (upper) and oxygen (lower) ions. The lowest panel presents the absolute value of the
439 DC magnetic field reported by the same instrument. A blue dashed line marks the start of
440 the EMIC-wave at 16:42 UT.

441
442

443

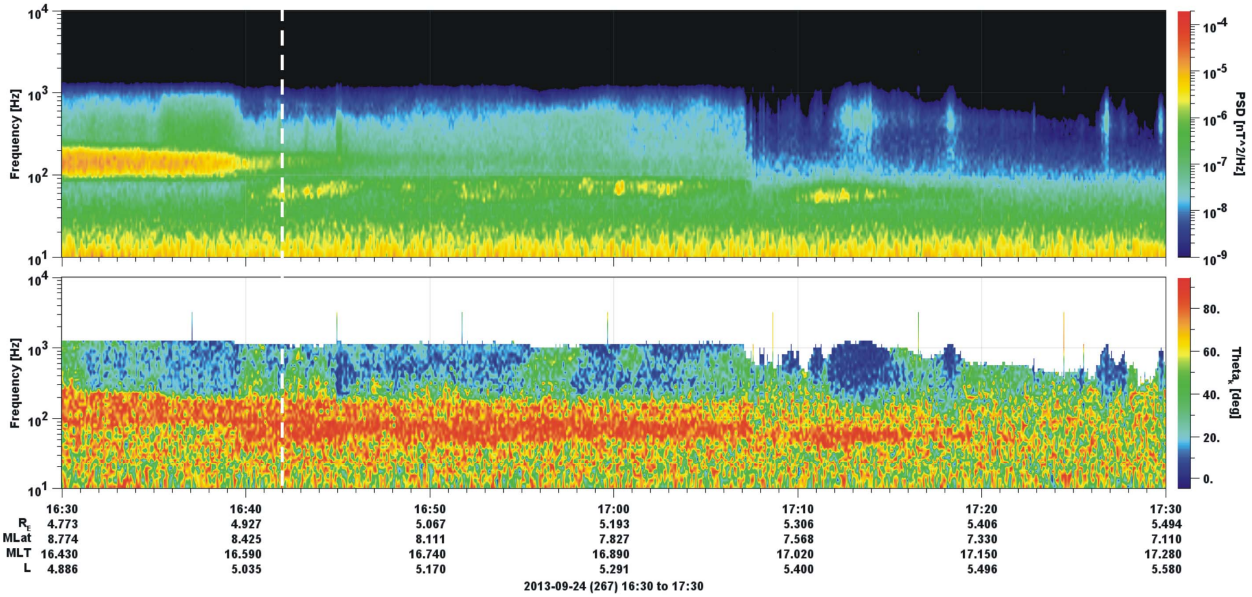

444

445 **Figure 2.** EMFISIS ELF/VLF magnetic field observations for the same time period shown
446 in Figure 1. The upper panel is the spectrogram of the summed magnetic field components
447 with units of nT^2/Hz. The lower panel shows the wave-normal angle with units of degrees,
448 determined from the upper panel waveforms.

449

450

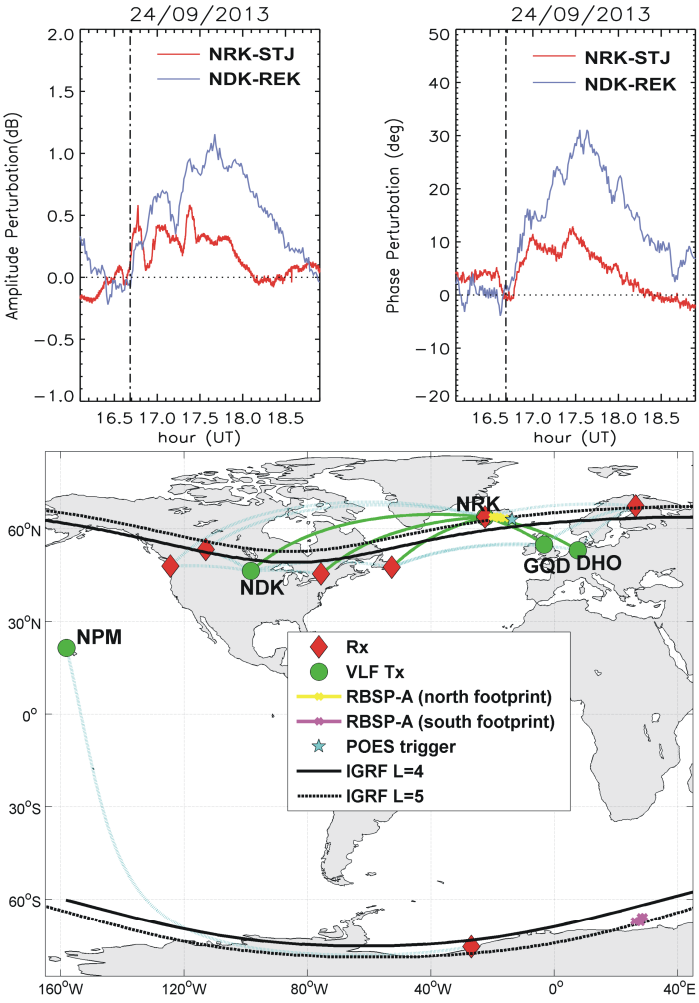

Figure 3. Summary of AARDDVARK observations at the event time. The upper panels shows amplitude and phase perturbations observed on the path NRK-St John's (Canada) (STJ, red) and NDK-Reykjavík (REK, blue). The black dashed line marks 16:42 UT. The lower panel is a map of the AARDDVARK paths analyzed in this study. RBSP-A northern (yellow) and southern (magenta) footprints are shown, as is the POES trigger sub-satellite point (blue star), AARDDVARK receivers (red diamonds), and VLF transmitters (green circles). In this plot AARDDVARK paths which were seen to respond to precipitation at the EMIC wave start time are shown in green, while the unresponsive paths are shown as dashed light blue lines.

461

462

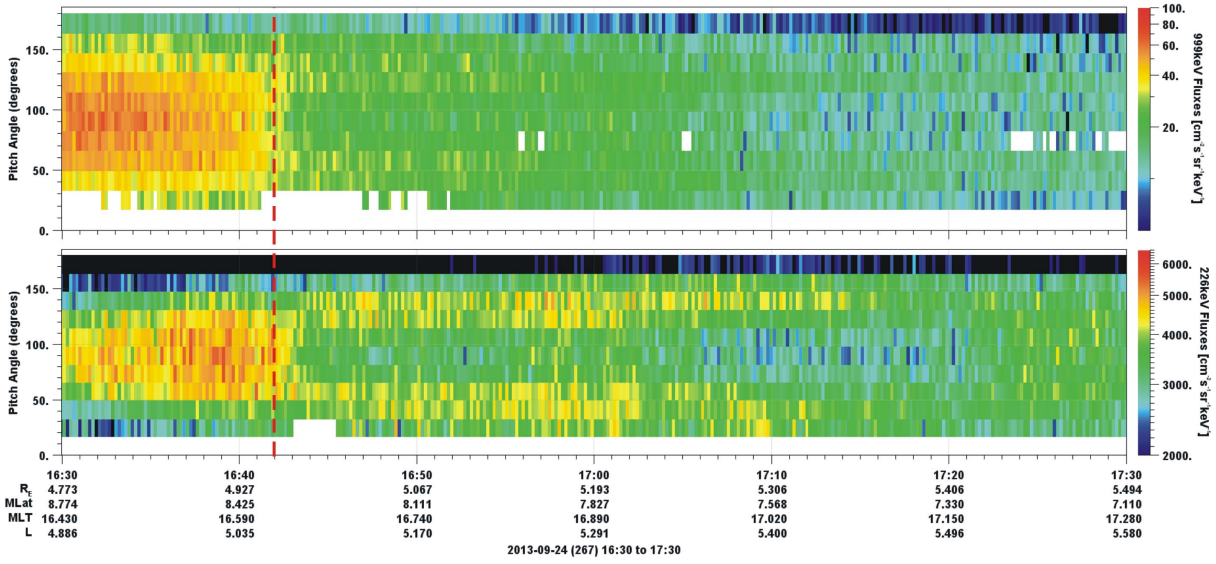

463

464 **Figure 4.** Butterfly pitch angle distributions seen in the MagEIS 1 MeV flux distributions

465 (upper panel) and the 225 keV distributions (lower panel). The dashed red line marks the

466 start of the EMIC wave seen in Figure 1.

467